recycling

MDPI

Article

Valorization of Sugarcane Bagasse Ash (SCBA) in Cementitious Composites: Hydration Behavior, Nanomodification and Sustainability Performance

Javier Rodrigo Nahuat-Sansores [1], Karla del Carmen García-Uitz [2], Julio César Cruz-Argüello [1,*], Carlos Andrés Ramírez-Pinto [1], Ricardo Enrique Vega-Azamar [1,*], Danna Lizeth Trejo-Arroyo [1] and Yazmin Vidal Valdez [3]

[1] Tecnológico Nacional de México/I. T. de Chetumal, Av. Insurgentes 330, Chetumal 77013, Q. Roo, Mexico; d14390332@chetumal.tecnm.mx (J.R.N.-S.); d12390316@chetumal.tecnm.mx (C.A.R.-P.); danna.ta@chetumal.tecnm.mx (D.L.T.-A.)

[2] SECIHTI—Tecnológico Nacional de México/I. T. de Chetumal, Av. Insurgentes 330, Chetumal 77013, Q. Roo, Mexico; karla.gu@chetumal.tecnm.mx

[3] División de Ingeniería en Nanotecnología, Instituto Tecnológico Superior de Ciudad Hidalgo, Av. Ing. Carlos Rojas Gutiérrez 2120, Fraccionamiento Valle de la Herradura, Ciudad Hidalgo 61100, Mich., Mexico; n21030449@itsch.edu.mx

* Correspondence: julio.ca@chetumal.tecnm.mx (J.C.C.-A.); ricardo.va@chetumal.tecnm.mx (R.E.V.-A.)

Abstract

Sugarcane bagasse ash (SCBA) has been widely studied as a partial supplementary cementitious material; nonetheless, its hydration behavior and performance when combined with nanoscale modifiers remain insufficiently understood. The aim of this study is to assess the pozzolanic potential of SCBA, the hydration behavior of binary SCBA–cement composites and the mechanical performance of ternary mortars with silica nanoparticles (Si-NPs). SCBA reactivity was confirmed by a Chapelle index of ~300 mg $Ca(OH)_2$/g, while hydration development in binary pastes (5–20 wt% SCBA) was quantified using TG/dTG and semi-quantitative XRD. Low SCBA replacement levels (5–10 wt%) enhanced the hydration degree by up to ~12% at 28 days compared with the reference paste. Ternary mortars incorporating 5 wt% SCBA and Si-NPs exhibited significant strength gains, with the optimal blend (2.5 wt% Si-NPs) achieving a 42% increase in 28-day compressive strength relative to the reference mortar. A sustainability assessment showed concurrent reductions in clinker intensity and CO_2 intensity of approximately 33% and 32%, respectively. These findings support the sustainable and technical viability of combining agro-industrial waste and nanotechnology as complementary strategies for reducing clinker content while enhancing eco-efficiency in alternative cementitious composites.

Keywords: sugarcane bagasse ash; hydration development; phase evolution; pozzolanic activity; nano-silica

Check for updates

Academic Editor: Denis Rodrigue

Received: 16 December 2025
Revised: 20 January 2026
Accepted: 27 January 2026
Published: 5 March 2026

Copyright: © 2026 by the authors. Licensee MDPI, Basel, Switzerland. This article is an open access article distributed under the terms and conditions of the Creative Commons Attribution (CC BY) license.

1. Introduction

The multi-component concrete based on Portland cement (PC) has been the leading product to accommodate the ever-increasing needs of worldwide expansion and urban infrastructure. Cement production is associated with an environmental burden generating between 7 and 10% of global CO_2 emissions [1]. One promising abatement strategy is the integration of supplementary cementitious materials (SCMs) into the cementitious compos-

ite design, reducing the clinker content while simultaneously enhancing the cementitious matrix [2].

Conventional SCMs, such as industrial by-products, including fly ash (FA), blast furnace ground slag (BFGS) and silica fume (SF), have been commercialized and used in a wide range of cement products throughout the years [3]; however, their supply and geographical scarcity due to the adoption of green policies in their respective industries presents a sizeable setback [4]. FA, and SF in particular, has been widely explored in the literature; for instance, the study of Golewski [5] explored the synergic effect of FA, SF and commercial nano-silica (nS) on the fracture behavior of modified concretes, observing an enhancement on brittleness and the fracture process on the SA + FA + nS concretes. Similarly, the study of Matos & Coutinho [6] investigated the effect of construction and demolition waste (CDW) and marble powder (MP) in both cement pastes and mortars, exhibiting a slightly decreased mechanical strength attributed to the low reactivity of the MP; however, workability and sustainability were improved. The authors emphasize the need to further optimize the CDW and MP as fillers.

In this context, agricultural residues have emerged as a promising solution in the face of these challenges, mainly due to the energy and resource savings associated with their production. Among these, sugarcane bagasse ash (SCBA) presents a unique opportunity to harness the pozzolanic potential of a by-product that requires little to no pre-treatment, ideal as a partial cement replacement [7]. Sugarcane bagasse incineration produces large quantities of ash, the final disposal of which is often open-air landfilling, resulting in a concerning eutrophication load which is environmentally concerning [8].

The synergy between SCBA and other admixtures has been of great interest in the literature [2] to further enhance the resulting cementitious composite. One such admixture consists of Si-NPs, which have been recognized for their ability to improve the cementitious microstructure as a consequence of enhanced pozzolanic activity and improved packaging. The NPs' sizes can range from 1 to 100 nm, exhibiting a high surface area that favors pozzolanic prominence. This combination of physical and chemical properties has proven to increase compressive strength and improve cohesion while reducing porosity [9,10].

The southeastern region of Mexico is a karstic zone characterized by limestone-rich soils and, consequently, high-calcium virgin materials. This geological condition presents a particular challenge for the construction industry in the production of mortars and concretes as excess calcium negatively affects the mechanical properties and durability. For instance, it can lead to reduced mechanical strength as it may cause improper reactions that impact the formation of hydration products (C-S-H). Additionally, limestone-rich materials tend to have higher porosity and capillarity, thus lower density, which facilitates water absorption in mortars. This high-water absorption not only affects mechanical strength but also allows external agents to penetrate and degrade the material [11–13].

This research aims to contribute to the existing body of research in SCBA and Si-NPs. Currently, several studies have addressed SCBA's influence on cementitious composite and its valuable contribution on energy reduction and waste minimization; nonetheless, the synergy between SCBA reinforced with Si-NPs in blends incorporating high-calcium aggregates has not been explored.

2. Results and Discussion

2.1. Microstructural Analysis, Mineralogic Profile and Pozzolanic Reactivity of SCBA and Calcareous Aggregates

Figure 1 presents the micrographs for SCBA at 500×, 1000× and 3000× scales. The microstructure predominantly appears irregularly shaped, typical of calcination via combustion. Certain crystalline structures are observed, such as the ones in (Figure 1a,b),

with mostly angular or sub-angular shapes, while no evidence of spherical morphology is observed, which is a particle shape typical of fly ash [7].

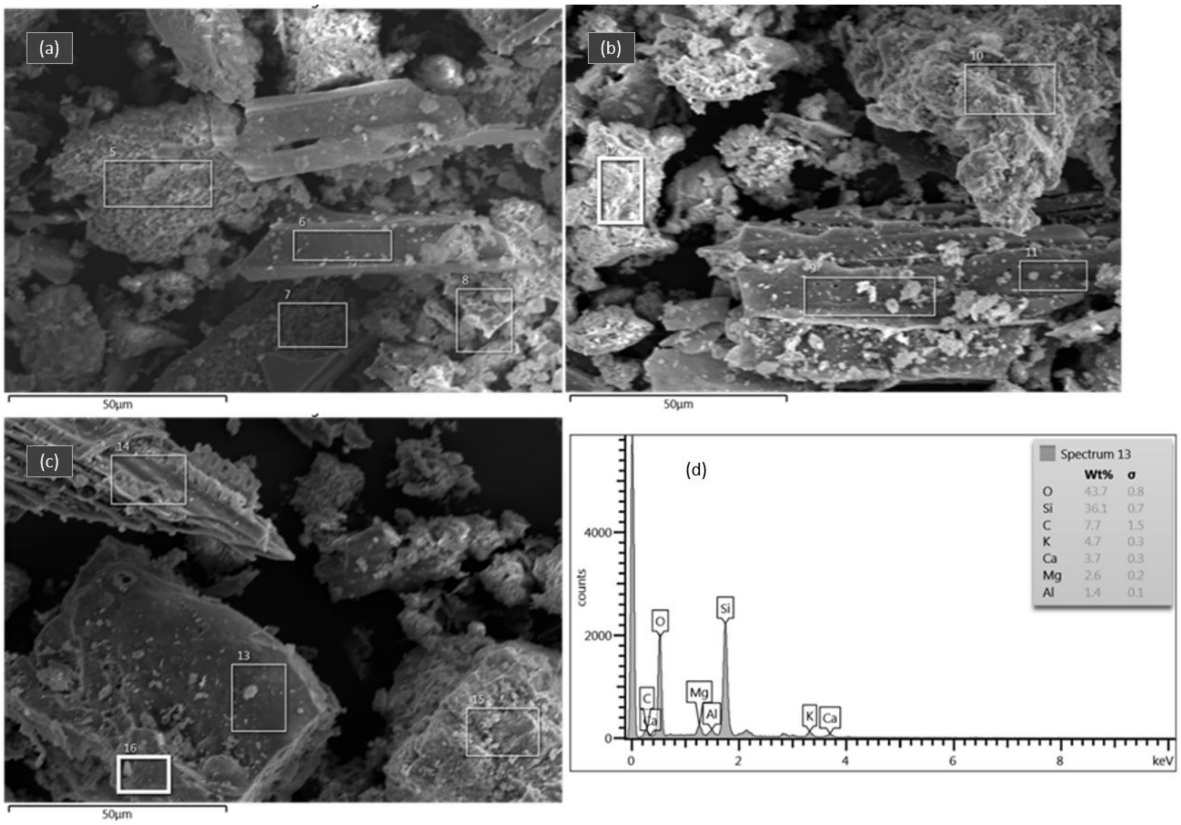


Figure 1. SEM micrographs of the SCBA sample at different magnifications: (**a**) 500×, (**b**) 1000×, (**c**) 3000× and (**d**) elemental composition by EDX analysis of the numbered areas in rectangles.

The surface texture appears rough and heterogenous, suggesting incomplete combustion at temperatures below 700 °C; beyond 800 °C, sintering occurs and crystalline phases dominate the microstructure, which is not the case for this uncontrolled combustion SCBA. This finding is also supported by the absence of crystalline phases such as well-formed quartz or distinctive $CaCO_3$/CaO crystals. Siliceous cellular and unburned carbon structure remnants can be observed in (Figure 1a,b), with rough surfaces, internal voids and porous structures. This distinctive porosity may enhance water retention while reducing density and mechanical strength development, adversely influencing the resulting cementitious composite. In (Figure 1c), a siliceous structure is highlighted and confirmed by the EDX analysis shown in (Figure 1d). The angular morphology and apparent high-surface area could indicate the potential for pozzolanic reactivity, which is also positively correlated with the amorphous silica content. However, the presence of larger unreactive particles (as the rough-surfaced ones mentioned in (Figure 1a,b)) may dilute reactivity. Therein lies the added value of nano-additive-mediated composites. The addition of Si-NPs could improve reactivity on two fronts: by increasing the available siliceous fraction and improving the packaging density.

In Figure 2, the chemical and elemental composition of the calcareous aggregates is observed. In (Figure 2a), its microstructure reveals a porous and heterogeneous surface, which certainly favors porosity and absorption. Calcareous aggregates are mainly composed of a blend of magnesium (Mg) and calcium carbonate ($CaCO_3$), also known as dolomite. Certain crystallite formations are observed that correspond to calcite and dolomite, as also confirmed by the EDX and XRD. (Figure 2b,c).

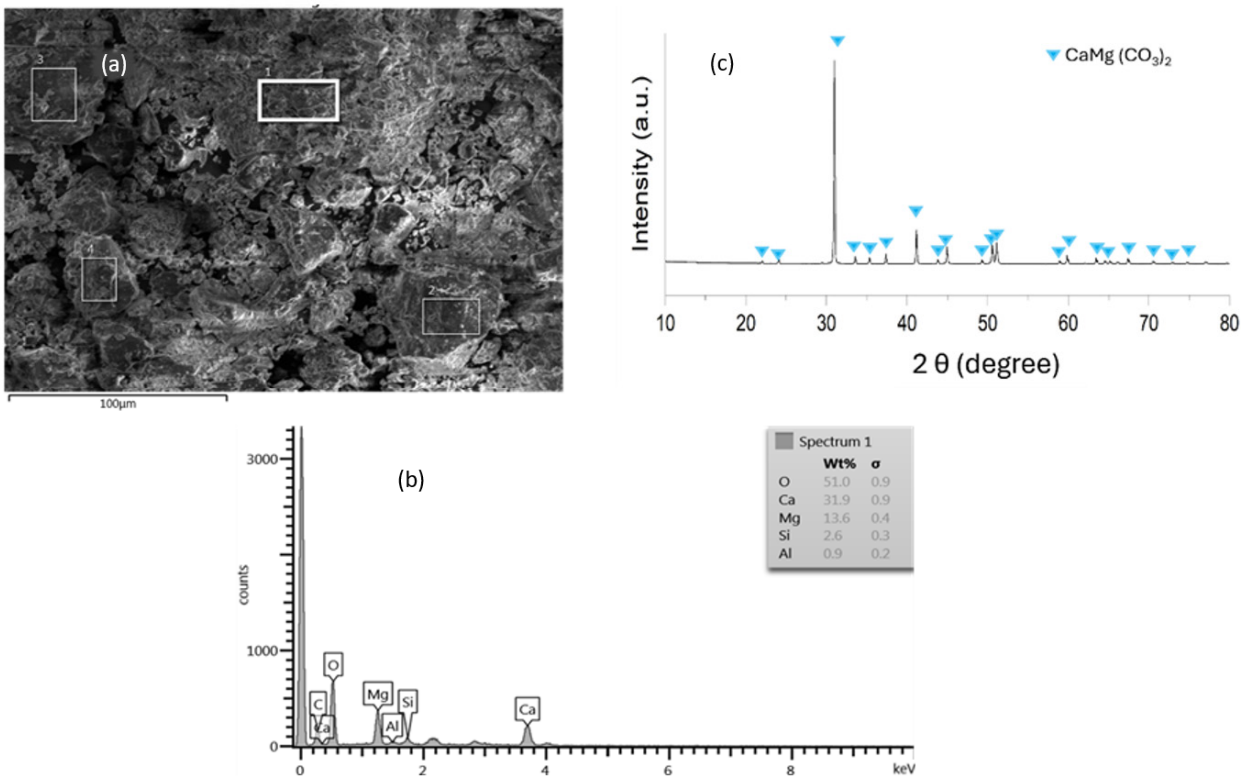


Figure 2. Calcareous aggregates: (**a**) microstructure via SEM, (**b**) elemental analysis via EDX and (**c**) mineralogical profile via XRD.

As observed in Figure 3, the mineralogic profile of SCBA displays several mineral compounds, including $CaCO_3$, SiO_2, Al_2O_3, FeO, Fe_2O_3 and an amorphous phase. The different diffraction peaks suggest SCBA is a semi-crystalline material, composed of calcite and ferro-siliceous components. The main diffraction peaks of the calcite component are 2θ = 23.022, 29.405 and 47.488°, while those of silicon dioxide (SiO_2) are 2θ = 31.205 and 50.147°. Notably, a wide band of dispersion between 15 and 30° 2θ angle is readily evident, corresponding to amorphous vitreous silicoaluminates, which may suggest potential pozzolanic activity.

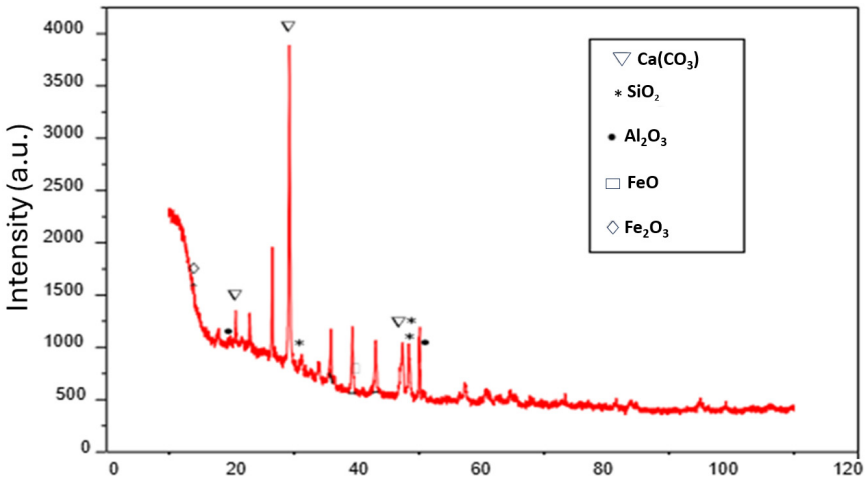


Figure 3. Mineralogic profile of SCBA.

In terms of pozzolanic reactivity, the SCBA sample obtained a Chapelle index of 299.99 mg/g of ash, ranging between 298 and 352 mg/g of ash, similar to the results obtained in the literature by other researchers [14]. For this test, the ash-free portlandite

was considered as the reference sample. All procedures concerning this test were carried out according to the French standard NF P 18-531 [15]. This test is designed to assess the $Ca(OH)_2$ consumption by the silicoaluminate phases; consequently, higher values indicate more $Ca(OH)_2$ consumption. Khan et al. [16] evaluated the pozzolanic potential of basaltic volcanic ash (VA) with different fineness levels and fly ash (FA) where VA obtained Chapelle values of 257.61 and up to 336.73 mg/g of sample, obtaining higher values for finer VA and FA obtained values of up to 666.27 mg/g of ash. For both SCBA and VA, the XRD diffractograms indicated significant amorphous silicoaluminate amorphous phases, while the pozzolanic activity test displayed a moderate amount of $Ca(OH)_2$ consumption. The reaction between silicoaluminate amorphous phases and calcium hydroxide leads to the formation of C-S-H, which would enhance the strength development via matrix densification.

2.2. Microstructural and Mineralogical Analysis of Si-NPs

Si-NPs were initially characterized via UV-vis (Figure 4a), which showed an absorbance peak at 298 nm, confirming the presence of Si-NPs in close agreement with previous results in the literature for Si-NPs synthetized by the sol–gel method [17]. The mineralogical profile via XRD also confirms the presence of Si-NPs by the characteristic amorphous halo due to the random packaging of SiO_4 (Figure 4b) in the 15–30° 2θ degrees. In the STEM image of (Figure 4c), certain agglomeration zones could be observed due to the development process of the Si-NPs, while a distinctive spherical shape is observed. Nanometric particles of sizes ranging from 22 to 36 nm could be distinguished, the observed average size is 30.7 nm (Figure 4d).

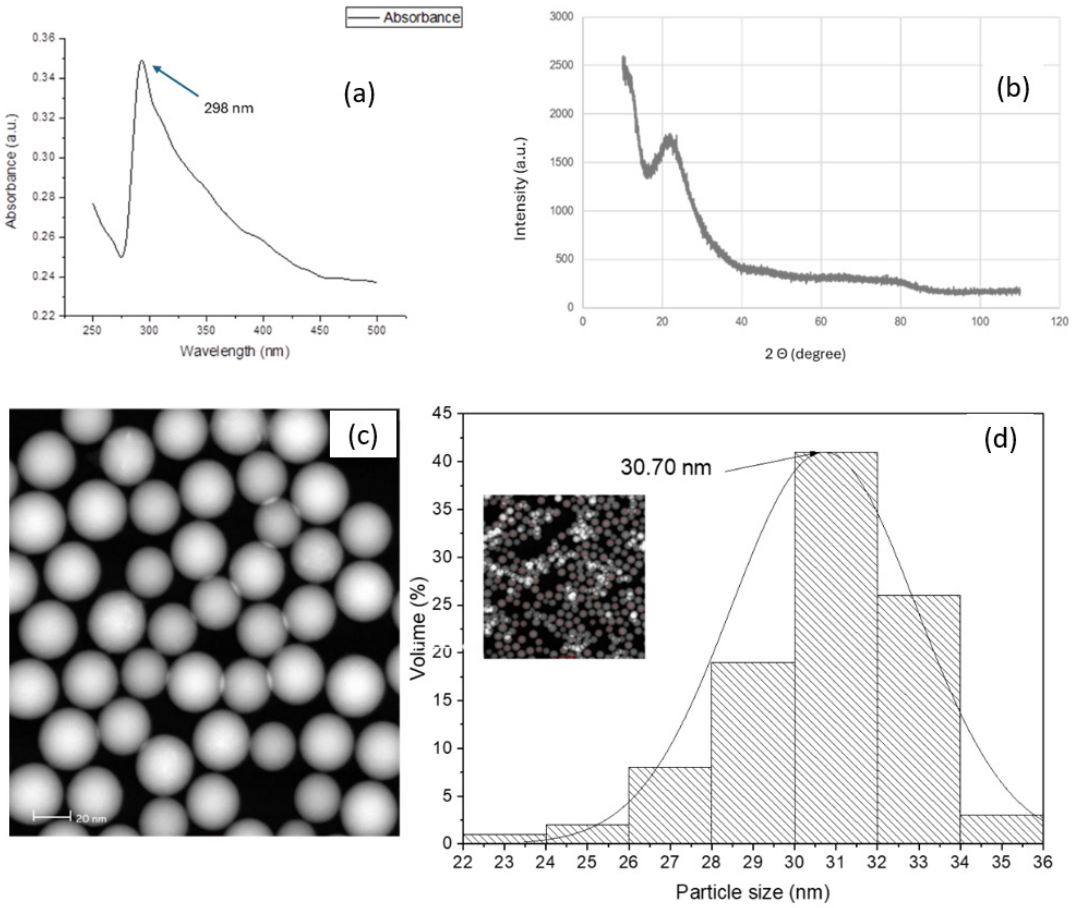


Figure 4. Characterization of the Si-NPs: (**a**) UV-visible spectrum, (**b**) x-ray diffraction pattern, (**c**) transmission electron microscopy image and (**d**) particle size analysis.

2.3. Hydration Degree (α) of Binary Cement Pastes

To study the hydration development of the complex SCBA cement system, binary cement pastes were evaluated at two different curing ages—7 and 28 days—for four different replacement ratios: 5, 10, 15 and 20 wt%; the TGA/dTG curves are shown in Figure 5 and the corresponding evolution of the hydration degree (α) is presented in Table 1.

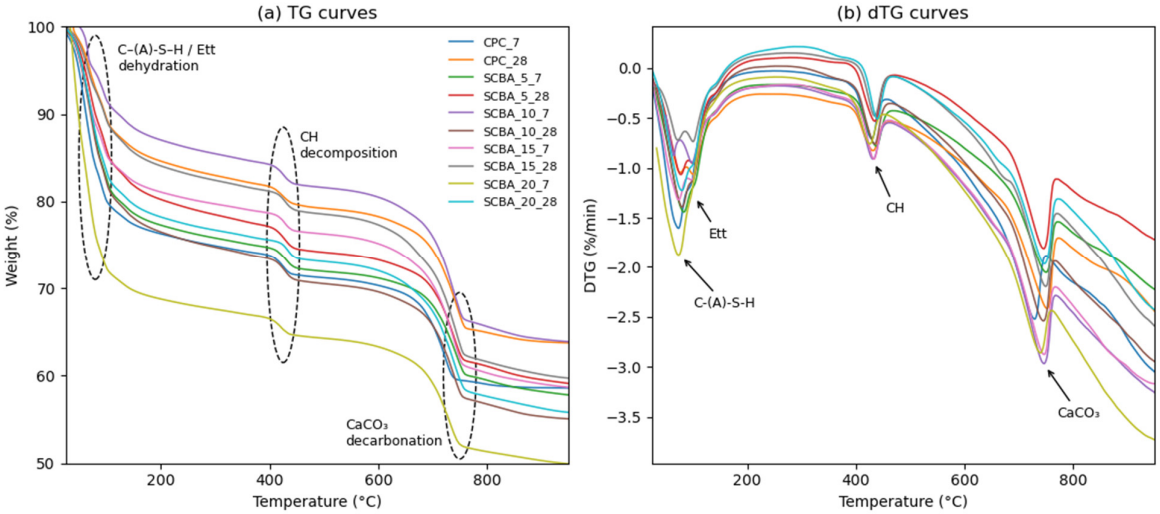


Figure 5. TG curves (**a**) and dTG curves (**b**) corresponding to the w/b = 0.5 binary cement pastes at the curing ages of 7 and 28 days.

Table 1. Hydration degree (α) and the bound water content (W_b) of the w/b = 0.5 binary cement pastes at the curing ages of 7 and 28 days.

Sample	Curing Age (Days)	Mass Loss %				Bound Water Content (W_b, %)	Hydration Degree (α, %)
		Ldh	Ldx	Ldc	L_{total}		
CPC 30R	7	7.971	1.058	12.043	21.072	13.967	58.19
	28	8.877	1.282	14.882	25.041	16.261	67.75
SCBA_5	7	8.982	1.223	13.846	24.051	15.882	66.17
	28	10.149	1.306	14.672	26.127	17.471	72.79
SCBA_10	7	8.889	1.326	17.074	27.289	17.215	71.73
	28	10.039	1.325	14.889	26.253	17.468	72.79
SCBA_15	7	7.968	1.278	16.973	26.219	16.205	67.52
	28	9.321	1.530	18.147	28.998	18.291	76.21
SCBA_20	7	7.125	1.086	13.878	22.089	13.901	57.92
	28	8.660	1.517	16.649	26.826	17.003	70.85

From (Figure 5a), the TG curves feature the three key thermal decomposition zones in cementitious composites: dehydration, dehydroxylation and decarbonation. The initial mass loss (<200 °C) corresponds mainly to the free water loss, the decomposition of ettringite (between 70 and 120 °C) and the partial decomposition of C-S-H [18]. As expected, all curves indicate a prominent mass loss at this temperature range; however, a greater loss is evident for SCBA blends at 28 days, attributed to the higher hydration products formed and the water absorbed by the pyrogenic ashes. In the dehydroxylation zone, portlandite decomposition is observed (between 400 and 500 °C). At 7 days, the reference cement samples exhibited a higher CH loss, implying more unreacted CH at that curing age. Conversely, SCBA blends (especially SCBA_10, SCBA_15 and SCBA_20) show less CH loss, indicating an enhanced pozzolanic reaction as the curing age increases, as

supported by SCBA pozzolanic activity in the Chapelle test. However, SCBA incorporation also increased the decarbonation of the composites due to the presence of $CaCO_3$ in the untreated sugarcane bagasse, which is evident for both 7 and 28 curing days and increases as the SCBA replacement ratio increases.

DTG peaks in (Figure 5b) reveal the rate of the mass loss, which is linked to specific hydration product decompositions. In the 100–200 °C range, C-S-H and ettringite decomposition shows stronger peaks for the SCBA samples, specifically for SCBA_5, SCBA_10 and SCBA_15. In the CH decomposition range between 400 and 450 °C, the peak is prominent in the reference curve at 7 days of curing, while at 28 days SCBA_5, SCBA_10 and SCBA_15 show reduced peaks, signaling effective pozzolanic reaction and secondary C-S-H formation. Accordingly, the last peak corresponds to the decarbonation of calcium phases. And as expected from the XRD and the TG profiles, as the content of SCBA increases the mass loss associated with decarbonation also increases.

The TG/dTG results indicate that SCBA incorporation modifies the hydration pathway of cement pastes by promoting early hydrate formation, reducing portlandite content through pozzolanic reactions and slightly increasing carbonate-related mass losses at elevated temperatures. These effects become more pronounced at 28 days, confirming the progressive reactivity of SCBA. Low-to-moderate replacement levels (5–10 wt%) appear particularly effective in enhancing hydration.

The evolution of the hydration degree (α) plays a key role in the development of hydration products and the reliability of supplementary cementitious materials. As shown in Table 1, the incorporation of untreated-SCBA as a replacement for cement influenced both the chemically bound water and the hydration degree at early (7 days) and later (28 days) ages.

Both parameters are closely associated with the evolution of the hydration phases and their reactions, leading to the formation of C-S-H gels and the consumption of (CH). All SCBA-blended pastes exhibited a progressive increase in the hydration degree. The reference cement paste achieved hydration degrees of 58.19% and 67.75% at 7 and 28 days, respectively. In contrast, all SCBA samples exhibited enhanced hydration at the same curing ages. While all SCBA samples exhibited greater hydration degrees than 70% above reference, substitutions up to 15 wt% provided optimal hydration degrees. Conversely, the SCBA_20 blend underperformed at 7 days and achieved an almost equal hydration degree as the reference. This effect is possibly due to the combination of dilution in the early age and the pozzolanic activity at later ages. The noticeable enhancement of SCBA-mediated blends is attributed to physical and chemical effects. In the former, the filler effect improved packaging and, in the latter, the pozzolanic activity promoted portlandite consumption and the production of extra C-S-H. These results suggest that SCBA incorporation as a cement replacement positively impacts hydration kinetics, particularly when incorporated at replacement levels between 5 and 15 wt%. Therein, balancing the enhancement due to pozzolanic activity/filler effect and the counteracting impact of clinker dilution is critical in order to develop optimal SCBA cementitious composites.

2.4. Phase Evolution of Binary Cement Pastes

The phase evolution via semi-quantitative X-ray diffraction (s-QXRD) analysis was performed to track the evolution of crystalline and amorphous phases as a proxy of the hydration kinetics occurring in the binary cement pastes over curing periods of 7 and 28 days. Valuable insight can be found within the kinetics of hydration that could well explain the clinker phase consumption (C_3S, C_2S) and the formation of stable phases, such as portlandite (CH) and ettringite (Ett) [19]. Table 2 presents the quantified phase assemblages observed for each blend across the studied curing ages.

Table 2. Phase evolution for the main hydration products of the w/b = 0.5 binary cement pastes at the curing ages of 7 and 28 days, according to the s-QXRD analysis.

Sample	C_3S	C_2S	$CaCO_3$	CH	Ettringite	Amorph.	Others *	Rwp	Rexp	X^2	GOF
CPC_7	0.66%	4.95%	19.96%	6.79%	7.51%	56.49%	3.64%	9.04	5.91	2.34	1.53
CPC_28	0.45%	4.17%	22.54%	8.12%	9.86%	50.02%	4.84%	8.31	4.13	4.05	2.01
SCBA_5_7	0.48%	7.49%	29.64%	8.27%	6.43%	42.10%	5.59%	8.64	5.94	2.12	1.45
SCBA_5_28	0.71%	4.39%	29.75%	7.15%	6.50%	45.17%	6.33%	8.01	4.12	3.78	1.94
SCBA_10_7	0.74%	6.24%	25.28%	7.22%	7.98%	46.60%	5.94%	9.06	5.84	2.41	1.55
SCBA_10_28	0.28%	4.68%	25.92%	8.84%	9.00%	44.50%	6.78%	7.84	4.15	3.57	1.89
SCBA_15_7	1.14%	6.79%	24.80%	7.03%	8.18%	46.53%	5.53%	7.85	4.07	3.72	1.93
SCBA_15_28	0.00%	4.27%	23.46%	7.92%	7.27%	49.99%	7.09%	7.68	4.01	3.67	1.92
SCBA_20_7	1.42%	7.36%	22.07%	8.33%	8.11%	46.40%	6.31%	7.99	4.08	3.84	1.96
SCBA_20_28	0.56%	3.84%	24.42%	7.33%	6.50%	51.00%	6.35%	8.54	4.03	4.49	2.12

* Others include minor detected phases such as gypsum, brownmillerite, monocarboaluminate, hemicarboaluminate and monosulfate.

The phase evolution determined by s-QXRD further corroborates the hydration degree (α) trends observed in the TG/dTG analysis. Minor fluctuations in residual clinker phases fall within the uncertainty of semi-quantitative Rietveld refinement and do not affect the observed trends. In the reference paste (CPC 30R), the clinker content decreases moderately (from 0.66% to 0.45% at 28 days of curing); simultaneously, the CH content increases. This is a typical and expected behavior of a composite Portland cement (CPC) with limited pozzolanic activity [20]. In contrast, high-replacement SCBA blends (15–20 wt%) exhibited more pronounced clinker depletion at 28 curing days compared with earlier curing ages; this effect could be explained by the cement dilution at earlier stages eventually offset by pozzolanic consumption at later curing ages. At low replacement levels (5–10 wt%), the clinker depletion behavior is similar to the reference cement; nonetheless, lower CH contents at 28 curing days are observed, consistent with the behavior observed in the TG/dTG analysis. This evidences the pozzolanic activity of SCBA by consuming CH to promote the formation of secondary hydration products. This effect is also evident for higher replacement levels (15–20 wt%) that increased their amorphous content, most likely due to the formation of secondary hydration products via pozzolanic activity across all curing ages. Similarly, the $CaCO_3$ content in all blends considers the replacement of moderate calcium cement replacement with another moderate calcium SCM. In the case of ettringite phases, these remained stable across all blends, signaling that the incorporation of SCBA did not disrupt the early sulfate stability. The findings of the s-QXRD corroborate the observed behavior in the TG/dTG and hydration degree (α) analyses, also confirming that low-to-moderate replacement levels (5–10 wt%) optimize hydration kinetics and phase evolution; conversely, excessive replacement (15–20 wt%) promotes dilution effects, significantly influencing the early hydration and ultimately offsetting the later pozzolanic benefits of SCBA incorporation.

2.5. Compressive Strength of Ternary (SCBA + Si-NPs) Mortar Blends

While the addition of Si-NPs to cement composites has been amply explored in the literature [17,21–23], the synergy between an untreated waste and these nanoparticles is of utmost interest for the cement research community, offering a new pathway to explore different combinations and to determine the right balance of strength, eco-efficiency and cost for this alternative cementitious blend. As discussed earlier, lower replacement levels (5–10 wt%) offer the most balanced profile between the dilution effects and pozzolanic gains by SCBA incorporation. Both SCBA and Si-NPs promote similar reactivity reactions, given that mechanical performance in mortars is particularly sensitive to clinker content and paste–aggregate interactions. The 5 wt% SCBA level was selected as the most representative

and conservative composition for assessing the synergistic effects of SCBA and Si-NPs for the compressive strength analysis at this second stage (ternary mortar blends), with two levels for the addition of Si-NPs: 1 and 2.5 wt% of SCBA. This approach ensured that the influence of Si-NPs could be evaluated under conditions where the binder matrix already exhibited optimized hydration behavior, thereby avoiding confounding effects related to excessive cement replacement. The compressive strength is presented in Figure 6.

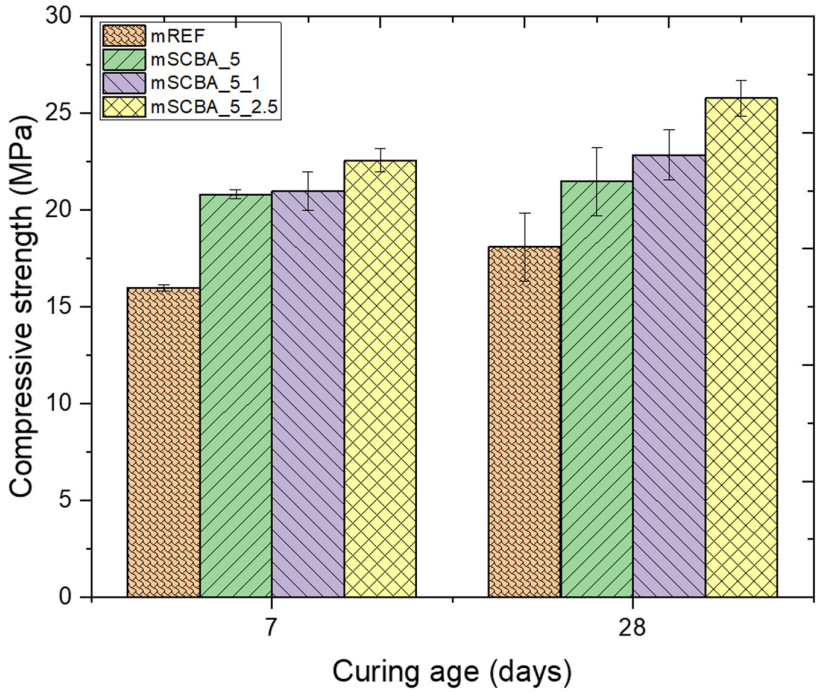


Figure 6. Compressive strength development for the ternary (SCBA + Si-NPs) mortar blends for 7- and 28-day curing ages.

The replacement of 5 wt% SCBA alone (mSCBA_5) improved strength in comparison with the reference mortar, aligning well with the hydration development trends observed in the s-QXRD and the hydration degree (α) analyses. At both 7 and 28 days, the mSCBA_5 blend outperformed the reference mortar, confirming the benefits of low replacement levels. As expected, incorporation of Si-NPs amplifies improvement further, possibly due to a denser microstructure and the extra C-S-H formation via additional nucleation sites [21,22,24]. mSCBA_5_1 yielded similar strength gains compared with mSCBA_5 at 7 days but outperformed this blend notably at 28 days. A slightly larger standard deviation is observed for the samples cured at 28 days, attributed mainly to the increased microstructural heterogeneity that develops with prolonged hydration and the number of replicate specimens (n = 3).

The highest achieved strength corresponds to the blend with the most addition of Si-NPs (2.5 wt%), with a considerable increase at 28 curing days. This enhancement is directly linked to the extra amorphous silica from Si-NPs, accelerating clinker consumption and consuming more CH, significantly influencing the late-age pozzolanic activity.

The synergy observed between SCBA and Si-NPs is attributed to the similar reaction pathways of each component. The former acts as a replacement material with pozzolanic benefits but dilution negative effects at high replacement levels, as observed in both the s-QXRD and TG/dTG analyses. Analogously, Si-NPs optimize particle packaging and provide additional amorphous-reactive silica; its morphology and mineral profile offer a unique combination that potentiates pozzolanic reactions at low addition levels (1 to 2.5 wt% in this study), thus easily overcoming the dilution negative impacts of SCBA

and calcium-rich aggregates. Simultaneous improvements in hydration kinetics, phase assemblage and, thus, compressive strength development can be delivered with a carefully tailored combination of SCBA and Si-NPs in cementitious composites.

2.6. Implications for High-Calcium Aggregate Composites

The results obtained in this study are particularly important for cementitious composites produced in regions with limestone-rich aggregates. In such composites, the excess availability of calcium can disrupt the balance between CH formation and C-S-H development, often leading to increased porosity, capillary connectivity and, thus, reduced mechanical performance [12]. The TG/dTG and s-QXRD results demonstrate that SCBA incorporation promotes the consumption of portlandite through pozzolanic reactions, thereby moderating the calcium-rich environment and favoring the formation of additional C–S–H. This effect is further enhanced by the presence of Si-NPs, which act as nucleation sites and accelerate the precipitation of finely distributed hydration products.

The observed improvements in compressive strength suggest that the combined SCBA/Si-NPs composites effectively compensate for the adverse effects associated with high-calcium aggregates by refining the microstructure and reducing the prevalence of weak, porous zones. Consequently, the proposed ternary blends offer a viable strategy to offset the mechanical challenges commonly associated with limestone-rich aggregate composites.

2.7. Eco-Efficiency Assessment Based on Compressive Strength and Clinker Content

The clinker intensity (CII) and CO_2-based intensity (COI) indices are metrics designed to assess the eco-efficiency of a cementitious composite per unit of strength, based on its clinker content reduction and its CO_2 abatements via clinker replacement. Therefore, lower CII and COI values equal lower emissions to deliver 1 MPa of compressive strength. These indices are derived from the studies of Damineli et al. [25], and the equations for the indices are as follows:

$$\mathrm{CII} = \mathrm{k}/\mathrm{cs} \quad (1)$$

$$\mathrm{COI} = \mathrm{c}/\mathrm{cs} \quad (2)$$

where k is the mass of clinker present per m^3 (kg clinker/m^3) and c is the GWP ($kgCO_2$-eq/m^3) of concrete for the selected life cycle stage. For this study, the chosen stages are A1-A3, for a cradle-to-gate analysis based on ISO 14040 [26] and ISO 14044 [27] standards. The corresponding data for the CII and COI indices are presented in Table 3 for a declared unit of 1 m^3 of mixed mortar. The only environmental impact considered in this study was the global warming potential (GWP) as it is considered the most influential for cementitious composites and the impact used as c in the COI calculation [25]. For CPC 30R, the GWP environmental impact was obtained from an EPD emitted by the cement company CEMEX® [28] (Yucatán Peninsula, Mexico), for the closest production plant. In the case of fine aggregates and water, values were obtained from a generic dataset from the European Life Cycle Database (ELCD) with denominations "Sand 0/2 mm, wet and dry quarry, production mix, at plant, undried RER S" and "Process water, production mix, at plant, ion exchange, from groundwater", respectively. SCBA is derived straight from the incineration at the sugar mill; therefore, it is treated as a "no allocation" waste as per ISO 14044 [27]. SCBA is a waste in the process; in this sugar mill sugarcane is grown and processed to produce sugar and energy. The alternative use case is the disposal of this waste via landfilling. Therefore, no upstream environmental burdens are allocated to SCBA according to the standard and the intended revalorization presented in this study. For the GWP of Si-NPs, a study detailing the impacts and contributions according to the synthesis

process is used as a proxy, as presented in Table 3. Despite the high embodied GWP of Si-NPs, their low dosage combined with significant strength gains results in net reductions in COI values.

Table 3. Constituents to obtain 1 m^3 of mortar, GWP per raw material and compressive strength of cubic samples at 28 curing days.

Sample	Constituents Per m^3 (kg)					CS_{28} (MPa)	Standard Deviation (MPa)
	Cement	F. Agg.	Water	SCBA	Si-NPs		
mREF	493.33	1356.67	346.40	0	0	18.11	1.76
mSCBA_5	468.67	1356.67	346.40	24.67	0	21.48	1.77
mSCBA_5_1	468.67	1356.67	346.40	24.67	0.25	22.86	1.29
mSCBA_5_2.5	468.67	1356.67	346.40	24.67	0.62	25.78	0.94

Raw Material	GWP ($kgCO_2$-eq/kg)	Reference	Source
Cement	0.777	[28]	CEMEX EPD
Fine Agg.	0.00246	[29]	ELCD 3.2
Water	0.00654	[29]	ELCD 3.2
SCBA	0	This study	This study
Si-NPs	12.59	[24]	Si-NPs from SCBA

From Table 3, each sample can obtain a derived GWP for the declared unit of 1 m^3. For mREF, mSCBA_5, mSCBA_5_1 and mSCBA_5_2.5 the GWP is 388.92, 369.76, 372.86 and 377.52 $kgCO_2$-eq/m^3, respectively. The corresponding CII and COI values are presented in Table 4 and Figure 7.

Table 4. GWP, clinker intensity (CII) and CO_2 indices (COI) for each sample in this study.

Sample	GWP ($kgCO_2$-eq/m^3)	CII (kgCement/m^3/MPa)	COI ($kgCO_2$/m^3/MPa)
mREF	388.92	21.17	21.48
mSCBA_5	369.76	16.95	17.21
mSCBA_5_1	372.86	15.93	16.31
mSCBA_5_2.5	377.52	14.13	14.64

Figure 7 presents the Damineli sustainability indices (CII and COI) for the four mixes of this study. The reference mix exhibits the lowest compressive strength and the highest CO_2 and clinker intensities. Partial clinker replacement with 5 wt% SCBA results in a clear rightward and downward shift, with lower CII and COI values (Figure 7a,b). This behavior signals simultaneous strength enhancement and reduction in environmental intensity. This demonstrates that even low SCBA substitution improves eco-efficiency relative to the 100% clinker system.

At constant SCBA replacement (5 wt%), the addition of Si-NPs further improves sustainability performance. Compared with mSCBA_5, both mSCBA_5_1 and mSCBA_5_2.5 achieve higher compressive strength while exhibiting lower CO_2 and clinker intensities. The progressive reduction in clinker intensity despite the increased compressive strength indicates that the nanoparticles enhance binder efficiency rather than increasing clinker demand. Among all mixes, mSCBA_5_2.5 attains the most favorable combination of mechanical performance and environmental efficiency.

In (Figure 7c), the relationship between CO_2 intensity and clinker intensity (COI and CII, respectively) shows a positive correlation, confirming clinker content as the primary driver of CO_2 emissions. Nonetheless, the displacement of NP-modified mixes toward the lower left region indicates that strength enhancement contributes to additional reductions

in environmental intensity per MPa beyond simple clinker substitution. Normalized indicators (Figure 7d) further confirm a systematic decrease in both COI and CII values from mREF to mSCBA_5_2.5, demonstrating that the combined use of SCBA and Si-NPs leads to a progressively improved mechanical sustainable balance.

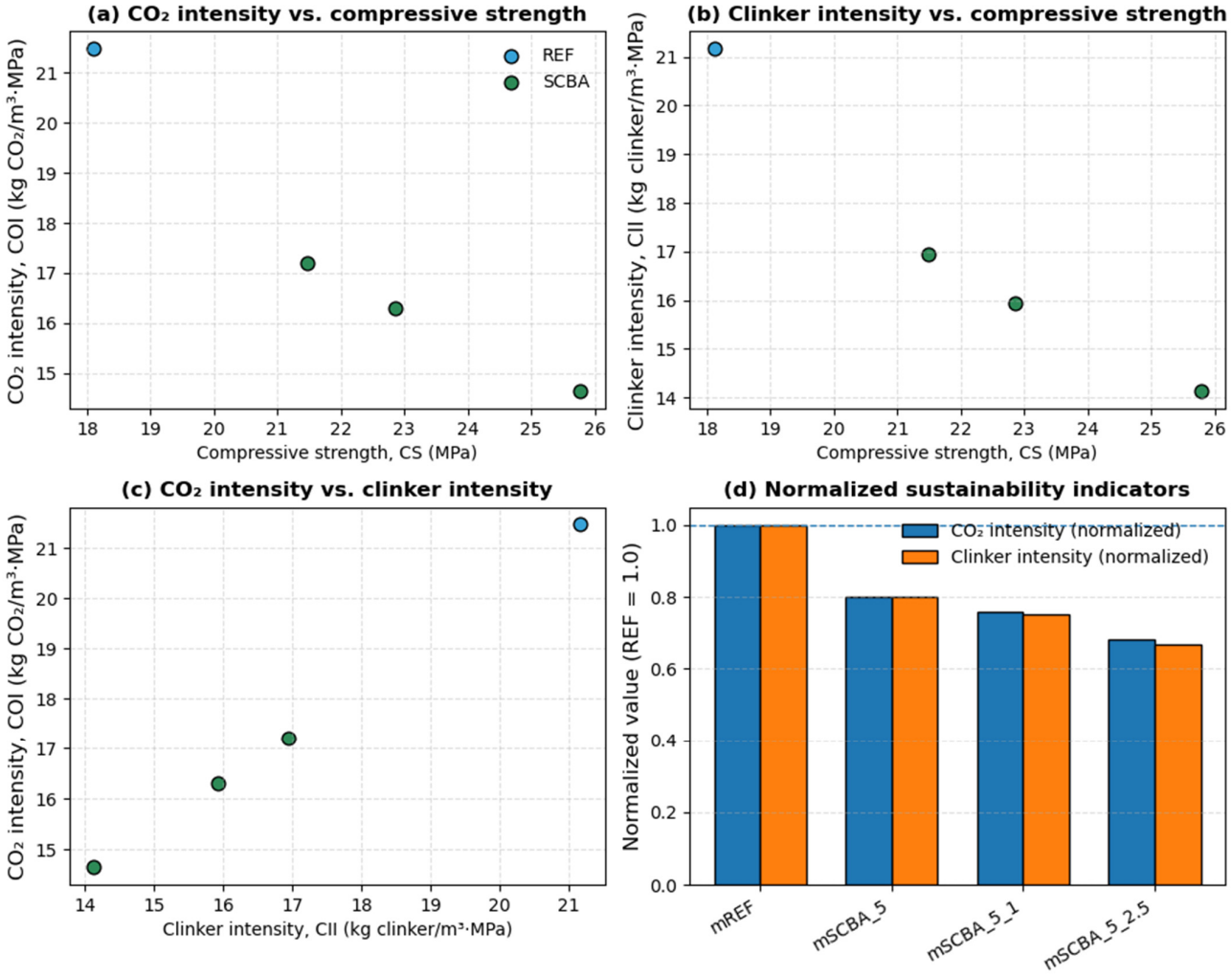


Figure 7. Sustainability indicators for the studied samples: (**a**) CO_2 intensity (COI) versus compressive strength at 28 curing days, (**b**) clinker intensity (CII) versus compressive strength at 28 curing days, (**c**) relationship between COI and CII and (**d**) normalized CO_2 intensity and clinker intensity relative to the reference mortar (mREF = 1.0). Lower values indicate improved eco-efficiency and clinker utilization.

3. Materials and Methods

3.1. Materials, Mix Proportion and Characterization Techniques

Raw materials for this project were sourced locally as follows: calcareous aggregates were sourced from a local quarry site; SCBA was collected at the "San Rafael Pucté" sugar mill (Yucatán Peninsula, Mexico) with an estimated capacity of nine thousand tons of sugarcane bagasse produced yearly; a composite Portland cement (CPC 30R, from CEMEX, Yucatán Peninsula, Mexico); complying with Type I of ASTM C150-22 [30] and Mexican standards for cement manufacturing [31]) served as the reference binder material due to commercial availability; the synthetized Si-NPs for this study were obtained by the sol–gel method as described below.

SCBA and calcareous aggregates were subjected to morphological analysis by SEM in a TESCAN Vega3 (Brno, Czech Republic), and elemental analysis was carried out with

the equipped energy-dispersive X-ray (EDX) from the same manufacturer (Brno, Czech Republic). Furthermore, the mineralogy of both SCBA and calcareous aggregates was determined by X-ray diffraction (XRD), by means of a Malvern PANalytical Empyrean Series 3 (Malvern, UK) with operating conditions of 40 kV and 30 mA in a Bragg–Brentano configuration, for 2θ values of 10–110°. Additionally, SCBA was subjected to the Chapelle pozzolanic activity test, as described in a previous study by the authors [32] and the provisions outlined in the French standard NF P 18-531 [15].

Silicon dioxide nanoparticles (Si-NPs) were synthetized by the sol–gel method, consisting of dissolving the molecular precursor in alcohol to convert it to gel by a combination of heating and stirring, also known as the "wet chemical method" [33]. For the Si-NPs in this study, 27.7 mL of tetraethyl orthosilicate (TEOS) was dissolved in 412.5 mL of absolute ethanol, following a procedure of stirring for 20 min. Simultaneously, 162 mL of distilled water and 19.2 mL of ammonium hydroxide were dissolved and stirred for 5 min. Thereafter, both solutions were mixed and stirred for 1 h at 40 °C and the solvent evaporated at 75 °C.

In order to remove impurities, the newly formed gel was centrifuged and washed with 95% ethanol and distilled water. The gel was finally dried in a MARLA aerated oven (Chetumal, Mexico) at 70 °C for 1 h, obtaining the Si-NPs. The resulting NPs were characterized by X-ray diffraction (XRD) and transmission electron microscopy (STEM) at 200 kV on a Philips Tecnai F20 (Tokyo, Japan) to obtain its mineralogic profile and to observe the morphology and distribution of the nanoparticles. Thereon, the average diameter of the resulting NPs was calculated.

The potential of SCBA and Si-NPs as supplementary cementitious materials (SCMs) was evaluated in two different stages: in binary cement pastes, where the influence of the untreated SCBA acting as a pozzolanic material was explored; secondly, the compressive strength was assessed in ternary mortars with the addition of Si-NPs.

In the case of cement pastes, four replacement ratios of SCBA were explored—5, 10, 15 and 20 wt% for a w/b ratio of 0.5—and tested at the curing ages of 7 and 28 days. In order to elucidate the SCBA influence on hydration development, two techniques were considered: thermogravimetric analysis (TGA/dTG) and semi-quantitative X-ray diffraction (s-QXRD). The samples were stored in laboratory conditions for curing (25 ± 2 °C and 60 ± 10% relative humidity) until the testing age and no hydration stoppage method was used. The TGA/dTG analysis was carried out in a TA SDT650 (New Castle, DE, USA) with samples weighting 20 ± 5 mg, in a N_2 atmosphere and a flux of 100 mL/min; the equipment resolution was 0.1 μg and ±0.5 °C. The associated weight loss was evaluated from room temperature up to 1000 °C, with a heating ramp of 10 °C/min. Analogously, semi-quantitative X-ray diffraction (s-QXRD) was carried out in a D8 Advance (Bruker, Ettlingen, Germany) at operating conditions of 40 kV and 40 mA, with a CuKα anode, exposition time of 1.2 s every 0.02°/s for a 2θ range of 7–75° in a Bragg–Brentano configuration. As an internal standard, high-purity anatase (>99%, Fermont) was used at a 9:1 ratio. Profex [34] software (v. 5.2.5) was used for the Rietveld analysis. Due to the binary nature of the cement pastes, the following nomenclature was adopted: REF, SCBA_5, SCBA_10, SCBA_15 and SCBA_20, according to the replacement ratio.

For the ternary mortar blends of the second stage (SCBA and Si-NPs), the provisions of ASTM C-109 [35] were considered. Three mortar specimens were manufactured per blend and four blends were considered for this stage: reference (mREF, 100% CPC 30R); a 5 wt% SCBA replacement ratio (mSCBA_5); a 5 wt% replacement ratio and a 1% Si-NPs addition (mSCBA_5_1) on a SCBA wt% basis; and a 5 wt% SCBA replacement with a 2.5 wt% Si-NPs addition (mSCBA_5_2.5) on a SCBA wt% basis. Figure 8 presents a flowchart for the experimental stage of this study.

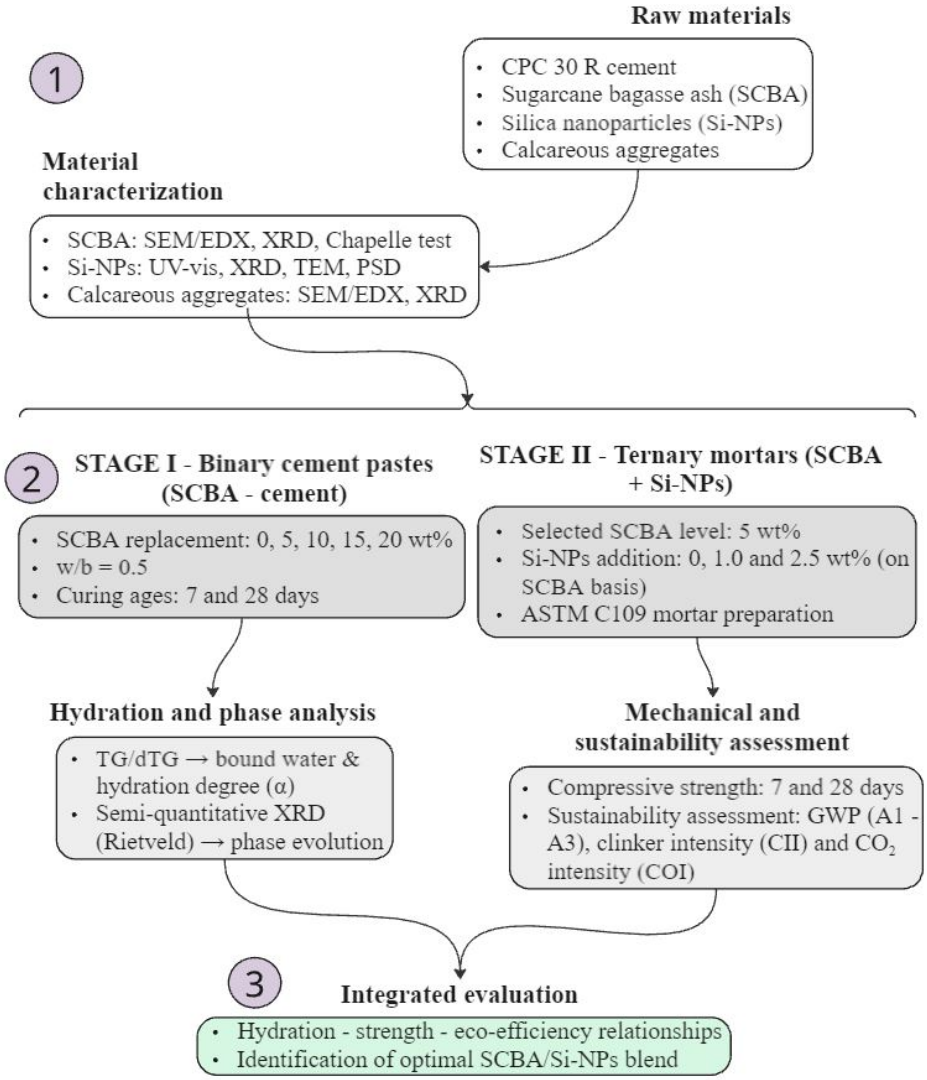


Figure 8. Flowchart of the experimental methodology adopted in this study, illustrating the two-stage approach.

3.2. Experimental Methodology

3.2.1. Determination of the Degree of Hydration (α) by TGA/dTG

The thermal decomposition of cementitious hydrates is characterized by descending values on the TGA curves. Generally, the three major phases of decomposition are classified as follows: a phase between 25 and 400 °C that represents evaporable water, a second phase between 400 and 600 °C corresponding to the dehydroxylation of calcium hydroxide and the last phase between 600 °C and 800 °C that corresponds to decarbonation; these values may vary slightly depending on the author and the study considerations [36]. The Bhatty method has been amply adopted in the literature for its ease of applicability and describes the hydration degree of cement pastes as explained by the following equations:

$$W_B = Ldh + Ldx + 0.41\ (Ldc) \quad (3)$$

$$\alpha = W_B/0.24 \quad (4)$$

where Ldh, Ldx and Ldc correspond to the relative mass losses on each dehydration, dehydroxylation and decarbonation decomposition phase, respectively. The WB factor is the chemically bound water at a given time t. Equation (4) defines the value 0.24 as the

chemically bound water at infinite time. Bhatty [37,38] considers the following ranges: 105–440 °C for Ldh, 440–580 °C for Ldx and 580–1000 for Ldc.

3.2.2. Phase Evolution Determined by s-QXRD

The evolution of the hydrates formed was determined by the Rietveld method [39] to quantitatively analyze the crystalline and amorphous phases. As mentioned above, SiO_2 (anatase) was employed as the internal standard to determine both amorphous and crystalline phases. Phases were identified according to the literature and databases; thus, relative proportions of amorphous and crystalline phases were obtained. The crystalline phases are summarized in Table 5, obtained from the literature and based upon available databases.

Table 5. Crystalline phases for the s-QXRD Rietveld method.

Crystalline Phases	Formula	Reference
Alite	C_3S	[40]
Belite	C_2S	[40]
C_3A_{Cubic}	C_3A	[41]
Calcite	$CaCO_3$	[42]
Gypsum	$CaSO_4{\cdot}2H_2O$	[43]
Ettringite	$C_3A{\cdot}3CaSO_4{\cdot}32H_2O$	[44]
Brownmillerite	C_4AF	[45]
Monosulfate	$C_3A{\cdot}CaSO_4{\cdot}xH_2O$	[46]
Monocarbonaluminate	$C_3A{\cdot}CaCO_3{\cdot}xH_2O$	[47]
Hemicarboaluminate	$C_3A{\cdot}Ca[(OH)(CO_3)_{0.5}]{\cdot}xH_2O$	[48]
Portlandite	$Ca(OH)_2$	[49]
Anatase	TiO_2	[50]

4. Conclusions

This study investigated the influence of a thermally activated untreated waste, such as SCBA, coupled with the addition of Si-NPs for the development of an alternative and eco-efficient cement composite. The influence of each component was assessed in two stages, first with SCBA as a replacement material in binary cement pastes and then as a ternary composite in mortars. The following key findings can be drawn from this study:

- Untreated SCBA exhibited moderate pozzolanic activity, as evidenced by the Chapelle index of ~300 mg $Ca(OH)_2/g$ and the reduced portlandite content in both s-QXRD and TG/dTG analyses, particularly at 28 days.
- Low SCBA replacement levels (5–10 wt%) provided the most balanced hydration development, increasing the degree of hydration by up to ~10–12% at 28 days compared with the reference, without compromising strength development via cement dilution.
- The highest addition of Si-NPs (2.5 wt%) yielded the best mechanical performance at 28 days, while SCBA alone at a low replacement (5 wt%) outperformed the reference, an increase of ~40% at 28 days relative to the reference mortar.
- From a sustainability perspective, the combined use of 5 wt% SCBA and Si-NPs significantly improved eco-efficiency indicators, achieving concurrent reductions of approximately 30–35% in clinker intensity and CO_2 intensity while delivering higher compressive strength.
- Among all the mixtures, the mSCBA_5_2.5 blend exhibited the most favorable balance between mechanical performance and environmental impact.

Overall, the synergistic use of SCBA and Si-NPs represents a viable pathway for producing low clinker cement composites, also demonstrating that agro-industrial waste

valorization coupled with nanomodification can effectively support the decarbonization of cementitious materials.

Author Contributions: J.R.N.-S.: conceptualization, writing—original draft, creation of models, editing, experiments. K.d.C.G.-U.: writing, editing, data acquisition. J.C.C.-A.: supervision, funding acquisition, writing—review and editing, project administration. C.A.R.-P.: experiments, data acquisition. R.E.V.-A.: conceptualization, writing—review and editing. D.L.T.-A.: microstructural analysis, data acquisition. Y.V.V.: conceptualization, data acquisition. All authors have read and agreed to the published version of the manuscript.

Funding: This research was funded by Tecnológico Nacional de México ("Estudio de la ceniza de bagazo de caña con adición de nanoesferas de SiO2 como material cementante suplementario (SCM) para compósitos base cemento, primera y segunda etapa"), grant numbers 20904.24-P and 22799.25-P.

Data Availability Statement: The original contributions presented in this study are included in the article. Further inquiries can be directed to the corresponding authors.

Acknowledgments: J.R.N.-S. and C.A.R.-P. acknowledge SECIHTI for the graduate scholarship granted. Likewise, K.d.C.G.-U. acknowledges SECIHTI for the postdoctoral scholarship granted.

Conflicts of Interest: The authors declare no conflicts of interest.

References

1. Lehne, J.; Preston, F. *Making Concrete Change: Innovation in Low-Carbon Cement and Concrete*; Chatham House Report; Chatham House: London, UK, 2018; pp. 1–122.
2. Tino Balestra, C.E.; Garcez, L.R.; Couto da Silva, L.; Veit, M.T.; Jubanski, E.; Nakano, A.Y.; Pietrobelli, M.H.; Schneider, R.; Ramirez Gil, M.A. Contribution to Low-Carbon Cement Studies: Effects of Silica Fume, Fly Ash, Sugarcane Bagasse Ash and Acai Stone Ash Incorporation in Quaternary Blended Limestone-Calcined Clay Cement Concretes. *Environ. Dev.* **2023**, *45*, 100792. [CrossRef]
3. Pal, S.C.; Mukherjee, A.; Pathak, S.R. Investigation of Hydraulic Activity of Ground Granulated Blast Furnace Slag in Concrete. *Cem. Concr. Res.* **2003**, *33*, 1481–1486. [CrossRef]
4. Chen, X.; Li, J.; Xue, Q.; Huang, X.; Liu, L.; Poon, C.S. Sludge Biochar as a Green Additive in Cement-Based Composites: Mechanical Properties and Hydration Kinetics. *Constr. Build. Mater.* **2020**, *262*, 120723. [CrossRef]
5. Golewski, G.L. Investigating the Effect of Using Three Pozzolans (Including the Nanoadditive) in Combination on the Formation and Development of Cracks in Concretes Using Non-Contact Measurement Method. *Adv. Nano Res.* **2024**, *16*, 217–229. [CrossRef]
6. Matos, A.M.; Coutinho, J.S. Binary and Ternary Blends of Construction and Demolition Waste and Marble Powder as Supplementary Cementitious Materials. *Sustainability* **2025**, *17*, 10769. [CrossRef]
7. Kolawole, J.T.; Babafemi, A.J.; Fanijo, E.; Chandra Paul, S.; Combrinck, R. State-of-the-Art Review on the Use of Sugarcane Bagasse Ash in Cementitious Materials. *Cem. Concr. Compos.* **2021**, *118*, 103975. [CrossRef]
8. Yaseen, N. Exploring the Potential of Sugarcane Bagasse Ash as a Sustainable Supplementary Cementitious Material: Experimental Investigation and Statistical Analysis. *Results Chem.* **2024**, *10*, 101723. [CrossRef]
9. Sáez Del Bosque, I.F.; Martínez-Ramírez, S.; Blanco-Varela, M.T. FTIR Study of the Effect of Temperature and Nanosilica on the Nano Structure of C-S-H Gel Formed by Hydrating Tricalcium Silicate. *Constr. Build. Mater.* **2014**, *52*, 314–323. [CrossRef]
10. Vitharana, M.G.; Paul, S.C.; Kong, S.Y.; Babafemi, A.J.; Miah, M.J.; Panda, B. A Study on Strength and Corrosion Protection of Cement Mortar with the Inclusion of Nanomaterials. *Sustain. Mater. Technol.* **2020**, *25*, e00192. [CrossRef]
11. Muciño, A.; Vargas, S.; Pérez, N.A.; Bucio, L.; Orozco, E. The Influence of Fine Aggregates on Portland Cement Mortar Compressive Strength. *Results Mater.* **2021**, *10*, 100182. [CrossRef]
12. Carlos, A.; Masumi, I.; Hiroaki, M.; Maki, M.; Takahisa, O. The Effects of Limestone Aggregate on Concrete Properties. *Constr. Build. Mater.* **2010**, *24*, 2363–2368. [CrossRef]
13. Alhozaimy, A.M. Effect of Absorption of Limestone Aggregates on Strength and Slump Loss of Concrete. *Cem. Concr. Compos.* **2009**, *31*, 470–473. [CrossRef]
14. Rodier, L.; Bilba, K.; Onésippe, C.; Arsène, M.A. Study of Pozzolanic Activity of Bamboo Stem Ashes for Use as Partial Replacement of Cement. *Mater. Struct./Mater. Constr.* **2017**, *50*, 87. [CrossRef]
15. *Standard NF P 18-513*; Pozzolanic Addition for Concrete—Metakaolin—Definitions, Specifications and Conformity Criteria. AFNOR—Association Française de Normalisation: Saint-Denis, France, 2010; pp. 1–19.
16. Khan, K.; Amin, M.N.; Saleem, M.U.; Qureshi, H.J.; Al-Faiad, M.A.; Qadir, M.G. Effect of Fineness of Basaltic Volcanic Ash on Pozzolanic Reactivity, ASR Expansion and Drying Shrinkage of Blended Cement Mortars. *Materials* **2019**, *12*, 2603. [CrossRef]

17. Raheem, A.A.; Abdulwahab, R.; Ikotun, B.D.; Adetoro, E.A. Evaluation of the Strength Performance and Microstructural Properties of Different Based Metakaolin Blended Cements Containing Greenly Synthesized Nanosilica. *Discov. Appl. Sci.* **2024**, *6*, 239. [CrossRef]
18. Qoku, E.; Bier, T.A.; Westphal, T. Phase Assemblage in Ettringite-Forming Cement Pastes: A X-Ray Diffraction and Thermal Analysis Characterization. *J. Build. Eng.* **2017**, *12*, 37–50. [CrossRef]
19. Srivastava, S.; Cerutti, M.; Nguyen, H.; Carvelli, V.; Kinnunen, P.; Illikainen, M. Carbonated Steel Slags as Supplementary Cementitious Materials: Reaction Kinetics and Phase Evolution. *Cem. Concr. Compos.* **2023**, *142*, 105213. [CrossRef]
20. Ríos-Parada, V.; Jiménez-Quero, V.G.; Valdez-Tamez, P.L.; Montes-García, P. Characterization and Use of an Untreated Mexican Sugarcane Bagasse Ash as Supplementary Material for the Preparation of Ternary Concretes. *Constr. Build. Mater.* **2017**, *157*, 83–95. [CrossRef]
21. Althoey, F.; Zaid, O.; Martínez-García, R.; Alsharari, F.; Ahmed, M.; Arbili, M.M. Impact of Nano-Silica on the Hydration, Strength, Durability, and Microstructural Properties of Concrete: A State-of-the-Art Review. *Case Stud. Constr. Mater.* **2023**, *18*, e01997. [CrossRef]
22. Tabish, M.; Zaheer, M.M.; Baqi, A. Effect of Nano-Silica on Mechanical, Microstructural and Durability Properties of Cement-Based Materials: A Review. *J. Build. Eng.* **2023**, *65*, 105676. [CrossRef]
23. Yang, H.; Monasterio, M.; Zheng, D.; Cui, H.; Tang, W.; Bao, X.; Chen, X. Effects of Nano Silica on the Properties of Cement-Based Materials: A Comprehensive Review. *Constr. Build. Mater.* **2021**, *282*, 122715. [CrossRef]
24. Mamidi, V.; Katakojwala, R.; Mohan, S.V. Amorphous Nano-Silica from Sugarcane Bagasse Ash—Process Optimization, Characterization, and Sustainability Analysis. *Biomass Convers. Biorefin.* **2025**, *15*, 4059–4071. [CrossRef]
25. Damineli, B.L.; Kemeid, F.M.; Aguiar, P.S.; John, V.M. Measuring the Eco-Efficiency of Cement Use. *Cem. Concr. Compos.* **2010**, *32*, 555–562. [CrossRef]
26. *ISO 14040*; Environmental Management—Life Cycle Assessment—Principles and Framework. ISO: Geneva, Switzerland, 2006.
27. *ISO 14044*; Environmental Management—Life Cycle Assessment—Requirements and Guidelines. ISO: Geneva, Switzerland, 2006.
28. CEMEX; Sociedad Anónima Bursátil de Capital Variable. *Environmental Product Declaration (EPD) for Cement Products Produced by CEMEX*; Mérida Facility: Mérida, Mexico; Monterrey, Mexico, 2023.
29. GreenDelta. *ELCD v.3.2 LCA Database*; GreenDelta GmbH: Berlin, Germany, 2025. Available online: https://nexus.openlca.org/ (accessed on 6 January 2026).
30. *ASTM C150-22*; Standard Specification for Portland Cement. Advancing Standards Transforming Markets: West Conshohocken, PA, USA, 2022. [CrossRef]
31. *NMX-C-414-ONNCCE-2014*; Building Industry—Hydraulic Cements—Specifications and Testing Methods. ONNCCE: Ciudad de México, Mexico, 2014.
32. Nahuat-Sansores, J.R.; Cruz, J.C.; Escobar, B.; Gurrola, M.P.; Ramírez-Pinto, C.A.; Garcia-Uitz, K. Evaluation of the Pozzolanic Potential of Poultry Litter Ash Calcined at Different Temperatures as a Revalorized Biomass Waste. *ACS Sustain. Resour. Manag.* **2024**, *1*, 950–957. [CrossRef]
33. Bhagwat, A.D.; Sawant, S.S.; Ankamwar, B.G.; Mahajan, C.M. Synthesis of Nanostructured Tin Oxide (SnO2) Powders and Thin Films by Sol-Gel Method. *J. Nano-Electron. Phys.* **2015**, *7*, 7–10.
34. Doebelin, N.; Kleeberg, R. Profex: A Graphical User Interface for the Rietveld Refinement Program BGMN. *J. Appl. Crystallogr.* **2015**, *48*, 1573–1580. [CrossRef]
35. *ASTM C109-13*; Standard Test Method for Compressive Strength of Hydraulic Cement Mortars (Using-in. or [50-mm] Cube Specimens). ASTM: West Conshohocken, PA, USA, 2013.
36. Deboucha, W.; Leklou, N.; Khelidj, A.; Oudjit, M.N. Hydration Development of Mineral Additives Blended Cement Using Thermogravimetric Analysis (TGA): Methodology of Calculating the Degree of Hydration. *Constr. Build. Mater.* **2017**, *146*, 687–701. [CrossRef]
37. Wang, C.; Chazallon, C.; Braymand, S.; Hornych, P. Thermogravimetric Analysis (TGA) for Characterization of Self-Cementation of Recycled Concrete Aggregates in Pavement. *Thermochim. Acta* **2024**, *733*, 179680. [CrossRef]
38. Bhatty, J.I. Hydration versus Strength in a Portland Cement Developed from Domestic Mineral Wastes—A Comparative Study. *Thermochim. Acta* **1986**, *106*, 93–103. [CrossRef]
39. De la Torre, Á.G.; De Vera, R.N.; Cuberos, A.J.M.; Aranda, M.A.G. Crystal Structure of Low Magnesium-Content Alite: Application to Rietveld Quantitative Phase Analysis. *Cem. Concr. Res.* **2008**, *38*, 1261–1269. [CrossRef]
40. Tsurumi, T.; Hirano, Y.; Kato, H.; Kamiya, T.; Daimon, M. Crystal Structure and Hydration of Belite. *Ceram. Trans.* **1993**, *40*, 19–25.
41. Mondal, P.; Jeffery, J.W. The Crystal Structure of Tricalcium Aluminate, $Ca_3Al_2O_6$. *Acta Crystallogr. Sect. B* **1975**, *31*, 689–697. [CrossRef]
42. Markgraf, S.A.; Reeder, R.J. High-Temperature Structure Refinements of Calcite and Magnesite. *Am. Mineral.* **1985**, *70*, 590–600.
43. Comodi, P.; Nazzareni, S.; Zanazzi, P.F.; Speziale, S. High-Pressure Behavior of Gypsum: A Single-Crystal X-Ray Study. *Am. Mineral.* **2008**, *93*, 1530–1537.

44. Gatta, D.; Hålenius, U.; Bosi, F.; Cañadillas-Delgado, L.; Teresa Fernandez-Diaz, M. Minerals in Cement Chemistry: A Single-Crystal Neutron Diffraction 3 Study of Ettringite, $Ca_6Al_2(SO_4)_3(OH)_{12}{\cdot}27H_2O$. *Am. Mineral.* **2019**, *104*, 73–78. [CrossRef]
45. Redhammer, G.J.; Tippelt, G.; Roth, G.; Amthauer, G. Structural Variations in the Brownmillerite Series $Ca_2(Fe_2\text{-}XAlx)O_5$: Single-Crystal X-Ray Diffraction at 25 °C and High-Temperature X-Ray Powder Diffraction (25 °C ≤ T ≤ 1000 °C). *Am. Mineral.* **2004**, *89*, 405–420. [CrossRef]
46. Allman, R. Refinement of the Hybrid Layer Structure $(Ca_2Al(OH)_6)$ + $(12SO_4{\cdot}3H_2O)$. *Neues Jahrb. Für Mineral.-Monatshefte* **1977**, *1977*, 136–144.
47. François, M.; Renaudin, G.; Evrard, O. A Cementitious Compound with Composition $3CaO.Al_2O_3.CaCO_3.11H_2O$. *Acta Crystallogr. Sect. C* **1998**, *54*, 1214–1217. [CrossRef]
48. Runčevski, T.; Dinnebier, R.E.; Magdysyuk, O.V.; Pöllmann, H. Crystal Structures of Calcium Hemicarboaluminate and Carbonated Calcium Hemicarboaluminate from Synchrotron Powder Diffraction Data. *Acta Crystallogr. B* **2012**, *68*, 493–500. [CrossRef]
49. Desgranges, L.; Grebille, D.; Calvarin, G.; Chevrier, G.; Floquet, N.; Niepce, J.-C. Hydrogen Thermal Motion in Calcium Hydroxide: $Ca(OH)_2$. *Acta Crystallogr. Sect. B* **1993**, *49*, 812–817. [CrossRef]
50. Weirich, T.E.; Winterer, M.; Seifried, S.; Mayer, J. Structure of Nanocrystalline Anatase Solved and Refined from Electron Powder Data. *Acta Crystallogr. Sect. A* **2002**, *58*, 308–315. [CrossRef]

Disclaimer/Publisher's Note: The statements, opinions and data contained in all publications are solely those of the individual author(s) and contributor(s) and not of MDPI and/or the editor(s). MDPI and/or the editor(s) disclaim responsibility for any injury to people or property resulting from any ideas, methods, instructions or products referred to in the content.